Acta Mech 229, 3501–3515 (2018)
https://doi.org/10.1007/s00707-018-2177-4

ORIGINAL PAPER

Yang Li · Lianzhi Yang · Liangliang Zhang · Yang Gao

Size-dependent effect on functionally graded multilayered two-dimensional quasicrystal nanoplates under patch/uniform loading

Received: 10 February 2018 / Revised: 23 April 2018 / Published online: 1 June 2018

Abstract The nonlocal effect on functionally graded multilayered quasicrystal nanoplates is investigated. The functionally graded quasicrystal is assumed to be exponentially distributed along the thickness direction of the simply supported nanoplates. The exact solution for functionally graded multilayered two-dimensional quasicrystal nanoplates subjected to a patch loading on their top surfaces is derived using the extended nonlocal elastic theory, pseudo-Stroh formalism, and propagator matrix method. The patch loading is indicated by the form of a double Fourier series expansion. Numerical examples are presented to reveal the influences of patch size, nonlocal parameter, and stacking sequence on the phonon, phason, and electric fields.

1 Introduction

Since the significant discovery of the icosahedral quasicrystals (QCs) first from the diffraction image of rapidly cooled Al-Mn alloys in 1982, a new research field for solid-state physics has been opened [1]. Unlike crystals and noncrystals, QCs possess long-range orientational order and no translational symmetry [2]. According to the elastic energy theory of QCs [3], there are two elementary excitations of low-energy in QCs: phonon and phason fields. The phason field describes the local rearrangement of atoms in a unit cell, whereas the phonon field is similar to the field in crystals. The existence of the phason field increases the complexity of the study on the QCs compared with crystals. QCs in the real three-dimensional (3D) physical space can be seen as a projection of a periodic lattice in the higher dimensional mathematic space [4]. A two-dimensional (2D) QC is generated by projecting the periodic lattice at five-dimensional space to the physical space, in which atom arrangement is periodic along one direction and quasiperiodic in a plane vertical to the periodic direction [5].

Due to the quasiperiodic atomic structure of QCs, they own many desirable properties, such as high hardness, high wear resistance, low friction coefficients, low adhesion [6–9]. Moreover, piezoelectricity is

Y. Li
College of Engineering, China Agricultural University, Beijing 100083, China

Y. Gao (✉)
College of Science, China Agricultural University, Beijing 100083, China
E-mail: gaoyangg@gmail.com

Y. Li
Department of Mechanical and Power Engineering, Yingkou Institute of Technology, Yingkou 115014, China

L. Yang
School of Civil and Resource Engineering, University of Science and Technology Beijing, Beijing 100083, China

L. Zhang
Department of Civil Engineering and Engineering Mechanics, Columbia University, New York 10027, USA

also one physical property of QCs [10,11]. QCs are expected to be used as surface coatings and particulate-reinforcing phase for an alloy [12–14]. Intensive study focusing on QCs has been done, such as 2D [15–17] and 3D [18–20] problems in QCs. Li [21,22] obtained the thermoelastic and electric–elastic general solutions of a 1D QC using the rigorous operator theory. Fan et al. [23] used the extended displacement discontinuity method to analyze cracks in 1D QCs and obtained the fundamental solutions. Li and Liu [24] obtained the analytical solutions for a 2D decagonal QC plate with elliptic hole by using the Stroh-like formalism. Sladek et al. [25] utilized the meshless Petrov–Galerkin method to analyze the bending behavior of 1D QC plate. Waksmanski et al. [26] studied the dynamic response of layered 1D QC plates in terms of the pseudo-Stroh formalism.

Al-based alloys composed of nanoquasicrystalline particles embedded in an α-Al matrix have been developed in the last decade, which show excellent mechanical properties relative to nanocrystalline alloys [27,28]. The classical continuum theory is not applicable for the study of the mechanical behavior of the nanostructure because the finite range of interatomic and intermolecular forces cannot be neglected. Therefore, some non-classical continuum theories, such as the nonlocal elastic theory [29,30] and nonlocal strain gradient theory [31], and modified couple stress theory [32], are proposed to investigated the quantum size effect in nanostructures. Among these theories, Eringen's nonlocal elastic theory is well accepted and widely applied [33–35]. The nonlocal elastic theory assumes that the stress at a point is a function of strains at all points of the body, and introduces internal characteristic parameters into the constitutive relations to account for the size effect in nanostructures [36].

The layered nanoplates play an important role in nanostructures. However, the sharp change in the material properties of laminated composites at the interface between two adjacent layers may result in microcrack or delamination [37]. Functionally graded (FG) materials are proposed to reduce the interface effects in the layered system, whose material properties vary continuously along one direction [38]. Due to the advantages of FG materials, static [39,40] and dynamic analyses [41] of FG multilayered plates have aroused great interest. Combining the advantages of functionally graded materials and QCs, functionally graded QCs are expected to be used as coating of cooker, thermal barrier coating, and surface coating of engines [42,43]. FG QCs can not only reduce stress concentration problems at the interfaces of the layers, but also have good performance and meet most stringent requirements in engineering compared with traditional FG materials. To the best of the authors' knowledge, most of the previous works focus on the multilayered plates made of QCs [5,18,20,26], no literature is available for the analysis of FG layered QC nanoplates.

The present paper focuses on the quantum size effect on FG multilayered QC plates, which combines 2D QC constitutive behavior with nonlocal effect, piezoelectric effect, and exponent-law distribution of constitutive coefficients. The nanoplates are simply supported and subjected to patch loading on their top surfaces. Based on the extended nonlocal theory and pseudo-Stroh formalism [44], the exact solution for a single FG nanoplate is derived. Afterward, the propagator matrix method [44] is introduced to treat the multilayered case. The influences of patch size, nonlocal parameter and stacking sequence on stresses, displacements, electric potential, and electric displacements are fully discussed.

2 Problem description and basic equations

Consider an N-layered FG 2D QC nanoplate with one of the four corners on the bottom surface being the origin of the coordinate system, as shown in Fig. 1. Related to a fixed material coordinate system (x_1, x_2, x_3), the global one has the relations $(x, y, z) = (x_1, x_2, x_3)$. The dimensions of the simply supported nanoplate are $x \times y \times z = L_x \times L_y \times H$. The poling and periodic directions for the 2D piezoelectric QC are along the z direction, and $x-y$ plane is the quasiperiodic plane. The jth layer with thickness $h_j = z_{j+1} - z_j$ is bounded by the lower interface at $z = z_j$ and the upper interface at $z = z_{j+1}$. It follows that the bottom and top surfaces of the nanoplate are $z_1 = 0$ and $z_{N+1} = H$, respectively. The material properties of the nanoplate are assumed to be exponentially distributed along the z-direction, and the displacement and traction components along the interfaces of the layers are continuous.

According to Refs. [19,34,45], the nonlocal constitutive relations for 2D decagonal QCs with the point groups 10*mm*, 1022, 10/*mmm* can be written as

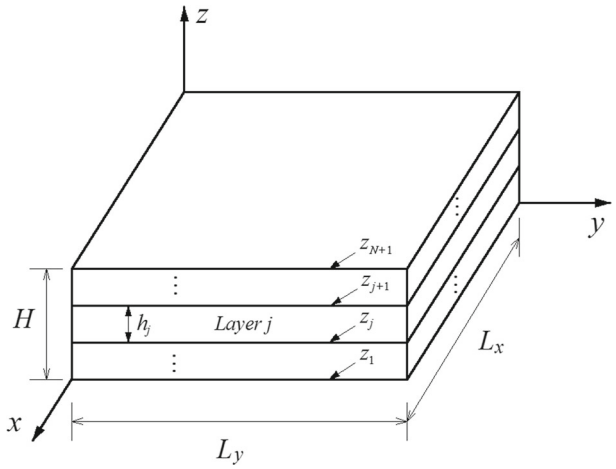

Fig. 1 An N-layered FG 2D QC nanoplate

$$
\begin{aligned}
&\left(1-l^2\nabla^2\right)\sigma_{11} = C_{11}\varepsilon_{11} + C_{12}\varepsilon_{22} + C_{13}\varepsilon_{33} + R_1(w_{11}+w_{22}) - e_{31}E_3,\\
&\left(1-l^2\nabla^2\right)\sigma_{22} = C_{12}\varepsilon_{11} + C_{11}\varepsilon_{22} + C_{13}\varepsilon_{33} - R_1(w_{11}+w_{22}) - e_{31}E_3,\\
&\left(1-l^2\nabla^2\right)\sigma_{33} = C_{13}\varepsilon_{11} + C_{13}\varepsilon_{22} + C_{33}\varepsilon_{33} - e_{33}E_3,\\
&\left(1-l^2\nabla^2\right)\sigma_{23} = \left(1-l^2\nabla^2\right)\sigma_{32} = 2C_{44}\varepsilon_{23} - e_{15}E_2,\\
&\left(1-l^2\nabla^2\right)\sigma_{31} = \left(1-l^2\nabla^2\right)\sigma_{13} = 2C_{44}\varepsilon_{13} - e_{15}E_1,\\
&\left(1-l^2\nabla^2\right)\sigma_{12} = \left(1-l^2\nabla^2\right)\sigma_{21} = 2C_{66}\varepsilon_{12} - R_1w_{12} + R_1w_{21},\\
&\left(1-l^2\nabla^2\right)H_{11} = R_1(\varepsilon_{11}-\varepsilon_{22}) + K_1w_{11} + K_2w_{22} - d_{112}E_2,\\
&\left(1-l^2\nabla^2\right)H_{22} = R_1(\varepsilon_{11}-\varepsilon_{22}) + K_1w_{22} + K_2w_{11} + d_{112}E_2,\\
&\left(1-l^2\nabla^2\right)H_{23} = K_4w_{23},\\
&\left(1-l^2\nabla^2\right)H_{12} = -2R_1\varepsilon_{12} + K_1w_{12} - K_2w_{21} - d_{112}E_1,\\
&\left(1-l^2\nabla^2\right)H_{13} = K_4w_{13},\\
&\left(1-l^2\nabla^2\right)H_{21} = 2R_1\varepsilon_{12} - K_2w_{12} + K_1w_{21} - d_{112}E_1,\\
&\left(1-l^2\nabla^2\right)D_1 = 2e_{15}\varepsilon_{13} + d_{112}(w_{12}+w_{21}) + \kappa_{11}E_1,\\
&\left(1-l^2\nabla^2\right)D_2 = 2e_{15}\varepsilon_{23} + d_{112}(w_{11}-w_{22}) + \kappa_{22}E_2,\\
&\left(1-l^2\nabla^2\right)D_3 = e_{31}(\varepsilon_{11}+\varepsilon_{22}) + e_{33}\varepsilon_{33} + \kappa_{33}E_3
\end{aligned}
\tag{1}
$$

where ∇^2 is the 3D Laplace operator; $l = e_0a$ is the nonlocal parameter, which shows the quantum size effect on the nanostructure, with a being the internal characteristic length and e_0 being a constant appropriate for each material; σ_{ij}, H_{ij}, and D_j represent the phonon stress, phason stress, and electric displacement, respectively; the phonon, phason, and phonon–phason coupling elastic coefficients are denoted by C_{ijkl}, K_{ijkl}, and R_{ijkl}, respectively; ε_{ij} and w_{ij} are the phonon and phason strains, respectively; the electric field intensity, permittivity constant, phonon piezoelectric constant, and phason piezoelectric constant are represented by E_k, κ_{ij}, e_{ijk}, and d_{ijk}, respectively; the subscripts obey the Einstein summation convention with $i, j, k, l = 1, 2, 3$.

In order to analyze functionally graded materials in an efficient manner, the material properties of FG 2D QCs are assumed to follow an exponential variation in the z-direction of the nanoplate and are given by [46]:

$$
\begin{aligned}
&C_{ijkl}(z) = C^0_{ijkl}\mathrm{e}^{\eta z}, \quad R_{ijkl}(z) = R^0_{ijkl}\mathrm{e}^{\eta z}, \quad K_{ijkl}(z) = K^0_{ijkl}\mathrm{e}^{\eta z},\\
&e_{ijk}(z) = e^0_{ijk}\mathrm{e}^{\eta z}, \quad d_{ijk}(z) = d^0_{ijk}\mathrm{e}^{\eta z}, \quad \kappa_{ij}(z) = \kappa^0_{ij}\mathrm{e}^{\eta z}
\end{aligned}
\tag{2}
$$

where η is the FG exponential factor denoting the degree of the material gradient in the z-direction, and the superscript '0' indicates material constants at the bottom surface for each layer of the FG multilayered nanoplate.

In the absence of body force and electric charge, the equilibrium equations are governed by [19]

$$
\sigma_{ij,j} = 0, \quad H_{ij,j} = 0, \quad D_{j,j} = 0. \tag{3}
$$

For 2D piezoelectric QCs, there are nonzero phonon displacements u_i ($i = 1, 2, 3$), and phason displacements w_1 and w_2. According to the 2D QC linear elastic theory [3], the gradient relations can be expressed as

$$
\varepsilon_{ij} = \left(u_{i,j} + u_{j,i}\right)/2, \quad w_{ij} = w_{i,j}, \quad E_j = -\phi_{,j}. \tag{4}
$$

3 General solution

For a simply supported FG multilayered 2D QC nanoplate, the general solution of the extended displacement vector is expressed as

$$\mathrm{u} = \begin{bmatrix} u_x \\ u_y \\ u_z \\ w_x \\ w_y \\ \phi \end{bmatrix} = \sum_{p,q} \mathrm{e}^{sz} \begin{bmatrix} a_1 \cos px \sin qy \\ a_2 \sin px \cos qy \\ a_3 \sin px \sin qy \\ a_4 \cos px \sin qy \\ a_5 \sin px \cos qy \\ a_6 \sin px \sin qy \end{bmatrix} \tag{5}$$

where

$$p = m\pi/L_x, \quad q = n\pi/L_y, \tag{6}$$

m and n are two positive integers, s and a_i ($i = 1, 2, \ldots, 6$) are the unknowns to be determined. Notice that the extended displacement vector satisfies the simply supported boundary conditions as follows:

$$\begin{aligned} &u_y = u_z = w_y = \phi = \sigma_{xx} = 0 \text{ at } x = 0 \text{ and } L_x, \\ &u_x = u_z = w_x = \phi = \sigma_{yy} = 0 \text{ at } y = 0 \text{ and } L_y. \end{aligned} \tag{7}$$

With the exponent-law-dependent material properties in Eq. (2), the extended traction vector is assumed as

$$\mathbf{t} = \begin{bmatrix} \sigma_{xz} \\ \sigma_{yz} \\ \sigma_{zz} \\ H_{xz} \\ H_{yz} \\ D_z \end{bmatrix} = \sum_{p,q} \mathrm{e}^{(s+\eta)z} \begin{bmatrix} b_1 \cos px \sin qy \\ b_2 \sin px \cos qy \\ b_3 \sin px \sin qy \\ b_4 \cos px \sin qy \\ b_5 \sin px \cos qy \\ b_6 \sin px \sin qy \end{bmatrix}. \tag{8}$$

The other in-plane stresses and electric displacements can be also derived as

$$\begin{bmatrix} \sigma_{xx} \\ \sigma_{xy} \\ \sigma_{yy} \\ H_{xx} \\ H_{yy} \\ H_{xy} \\ H_{yx} \\ D_x \\ D_y \end{bmatrix} = \sum_{p,q} \mathrm{e}^{(s+\eta)z} \begin{bmatrix} c_1 \sin px \sin qy \\ c_2 \cos px \cos qy \\ c_3 \sin px \sin qy \\ c_4 \sin px \sin qy \\ c_5 \sin px \sin qy \\ c_6 \cos px \cos qy \\ c_7 \cos px \cos qy \\ c_8 \cos px \sin qy \\ c_9 \sin px \cos qy \end{bmatrix}. \tag{9}$$

The three vectors

$$\begin{aligned} &\mathrm{a} = [a_1, a_2, a_3, a_4, a_5, a_6]^{\mathrm{T}}, \mathrm{b} = [b_1, b_2, b_3, b_4, b_5, b_6]^{\mathrm{T}}, \\ &\mathrm{c} = [c_1, c_2, c_3, c_4, c_5, c_6, c_7, c_8, c_9]^{\mathrm{T}} \end{aligned} \tag{10}$$

are introduced to denote the coefficients in Eqs. (5), (8), and (9). The superscript 'T' represents a vector or matrix transpose.

Utilizing the constitutive relation in Eq. (1), the relation between vectors **a** and **c** reads

$$\left[1-(e_0a)^2\left(s^2-p^2-q^2\right)\right]\begin{bmatrix}c_1\\c_2\\c_3\\c_4\\c_5\\c_6\\c_7\\c_8\\c_9\end{bmatrix}=\begin{bmatrix}-C_{11}^0p & -C_{12}^0q & C_{13}^0s & -R_1^0p & -R_1^0q & e_{31}^0s\\ C_{66}^0q & C_{66}^0p & 0 & -R_1^0q & R_1^0p & 0\\ -C_{12}^0p & -C_{11}^0q & C_{13}^0s & R_1^0p & R_1^0q & e_{31}^0s\\ -R_1^0p & R_1^0q & 0 & -K_1^0p & -K_2^0q & d_{112}^0q\\ -R_1^0p & R_1^0q & 0 & -K_2^0p & -K_1^0q & -d_{112}^0q\\ -R_1^0q & -R_1^0p & 0 & K_1^0q & -K_2^0p & d_{112}^0p\\ R_1^0q & R_1^0p & 0 & -K_2^0q & K_1^0p & d_{112}^0p\\ e_{31}^0s & 0 & e_{15}^0p & -d_{112}^0q & d_{112}^0p & -\kappa_{11}^0p\\ 0 & e_{15}^0s & e_{15}^0q & -d_{112}^0p & d_{112}^0q & -\kappa_{22}^0q\end{bmatrix}\begin{bmatrix}a_1\\a_2\\a_3\\a_4\\a_5\\a_6\end{bmatrix}. \tag{11}$$

Similarly, the relation between vectors **a** and **b** can be achieved by substituting Eq. (5) into Eqs. (4) and (1) as

$$\left[1-(e_0a)^2\left(s^2-p^2-q^2\right)\right]\mathbf{b}=\left(-\mathbf{P}^{\mathrm{T}}+s\mathbf{T}\right)\mathbf{a}=-\frac{1}{s+\eta}\left(\mathbf{Q}+s\mathbf{P}\right)\mathbf{a} \tag{12}$$

where

$$\mathrm{P}=\begin{bmatrix}0 & 0 & C_{13}^0p & 0 & 0 & e_{31}^0p\\ 0 & 0 & C_{13}^0q & 0 & 0 & e_{31}^0q\\ -C_{44}^0p & -C_{44}^0q & 0 & 0 & 0 & 0\\ 0 & 0 & 0 & 0 & 0 & 0\\ 0 & 0 & 0 & 0 & 0 & 0\\ e_{15}^0p & e_{15}^0q & 0 & 0 & 0 & 0\end{bmatrix},\quad \mathrm{T}=\begin{bmatrix}C_{44}^0 & 0 & 0 & 0 & 0 & 0\\ 0 & C_{44}^0 & 0 & 0 & 0 & 0\\ 0 & 0 & C_{33}^0 & 0 & 0 & e_{33}^0\\ 0 & 0 & 0 & K_4^0 & 0 & 0\\ 0 & 0 & 0 & 0 & K_4^0 & 0\\ 0 & 0 & e_{33}^0 & 0 & 0 & -\kappa_{33}^0\end{bmatrix}, \tag{13.1}$$

$$\mathbf{Q}=\begin{bmatrix}-\left(C_{11}^0p^2+C_{66}^0q^2\right) & -pq\left(C_{12}^0+C_{66}^0\right) & 0 & R_1^0\left(q^2-p^2\right) & -2R_1^0pq & 0\\ -pq\left(C_{12}^0+C_{66}^0\right) & -\left(C_{66}^0p^2+C_{11}^0q^2\right) & 0 & 2R_1^0pq & R_1^0\left(q^2-p^2\right) & 0\\ 0 & 0 & -C_{44}^0\left(p^2+q^2\right) & 0 & 0 & -e_{15}^0\left(p^2+q^2\right)\\ R_1^0\left(q^2-p^2\right) & 2R_1^0pq & 0 & -K_1^0\left(p^2+q^2\right) & 0 & 0\\ -2R_1^0pq & R_1^0\left(q^2-p^2\right) & 0 & 0 & -K_1^0\left(p^2+q^2\right) & -d_{112}^0\left(p^2+q^2\right)\\ 0 & 0 & -e_{15}^0\left(p^2+q^2\right) & 0 & -d_{112}^0\left(p^2+q^2\right) & \kappa_{11}^0p^2+\kappa_{22}^0q^2\end{bmatrix}. \tag{13.2}$$

Substituting Eqs. (8) and (9) into Eq. (3) yields the eigenequation as

$$\left[\mathbf{Q}-\eta\mathbf{P}^{\mathrm{T}}+s(\mathbf{P}-\mathbf{P}^{\mathrm{T}}+\eta\mathbf{T})+s^2\mathbf{T}\right]\mathbf{a}=\mathbf{0}. \tag{14}$$

In order to convert the quadratic equation (14) into a linear equation, the intermediate linear transformation vector **d** is introduced as

$$\mathbf{d}=\left(-\mathbf{P}^{\mathrm{T}}+s\mathbf{T}\right)\mathbf{a}=-\frac{1}{s+\eta}\left(\mathbf{Q}+s\mathbf{P}\right)\mathbf{a}. \tag{15}$$

With the aid of the intermediate linear transformation vector **d**, the standard eigenrelation can be obtained as follows:

$$\mathbf{N}\begin{bmatrix}\mathbf{a}\\\mathbf{d}\end{bmatrix}=s\begin{bmatrix}\mathbf{a}\\\mathbf{d}\end{bmatrix} \tag{16}$$

where

$$\mathbf{N}=\begin{bmatrix}\mathbf{T}^{-1}\mathbf{P}^{\mathrm{T}} & \mathbf{T}^{-1}\\ -\mathbf{Q}-\mathbf{P}\mathbf{T}^{-1}\mathbf{P}^{\mathrm{T}} & -\mathbf{P}\mathbf{T}^{-1}-\eta\mathbf{I}\end{bmatrix}. \tag{17}$$

The 12 eigenvalues s_i (i = 1, 2, …, 12) and the corresponding eigenvector **a** can be solved from Eq. (16). The eigenvectors **b** should be obtained from Eq. (12), which is different from the local case [20]. A subscript is

attached to eigenvectors **a** and **b** to distinguish them. Then, the general solution for the extended displacement and traction vectors is obtained as

$$\begin{bmatrix}\mathbf{u}\\ \mathbf{t}\end{bmatrix}=\begin{bmatrix}\mathbf{I} & \mathbf{0}\\ \mathbf{0} & \mathrm{e}^{\eta z}\mathbf{I}\end{bmatrix}\begin{bmatrix}\mathbf{A}_1 & \mathbf{A}_2\\ \mathbf{B}_1 & \mathbf{B}_2\end{bmatrix}\left\langle \mathrm{e}^{s^* z}\right\rangle\begin{bmatrix}\mathbf{D}_1\\ \mathbf{D}_2\end{bmatrix} \tag{18}$$

where

$$\begin{aligned}&\mathbf{A}_1=[\mathbf{a}_1,\ \mathbf{a}_2,\ \mathbf{a}_3,\ \mathbf{a}_4,\ \mathbf{a}_5,\ \mathbf{a}_6],\quad \mathbf{A}_2=[\,\mathbf{a}_7,\ \mathbf{a}_8,\ \mathbf{a}_9,\ \mathbf{a}_{10},\mathbf{a}_{11},\mathbf{a}_{12}],\\ &\mathbf{B}_1=[\mathbf{b}_1,\ \mathbf{b}_2,\ \mathbf{b}_3,\ \mathbf{b}_4,\ \mathbf{b}_5,\mathbf{b}_6],\quad \mathbf{B}_2=[\mathbf{b}_7,\ \mathbf{b}_8,\ \mathbf{b}_9,\ \mathbf{b}_{10},\ \mathbf{b}_{11},\ \mathbf{b}_{12}],\\ &\left\langle \mathrm{e}^{s^* z}\right\rangle=\mathrm{diag}\big[\mathrm{e}^{s_1 z},\ \mathrm{e}^{s_2 z},\ \mathrm{e}^{s_3 z},\ \mathrm{e}^{s_4 z},\ \mathrm{e}^{s_5 z},\ \mathrm{e}^{s_6 z},\ \mathrm{e}^{(-s_1-\eta)z},\ \mathrm{e}^{(-s_2-\eta)z},\ \mathrm{e}^{(-s_3-\eta)z},\ \mathrm{e}^{(-s_4-\eta)z},\\ &\quad \mathrm{e}^{(-s_5-\eta)z},\ \mathrm{e}^{(-s_6-\eta)z}\big],\end{aligned} \tag{19}$$

$\mathbf{D}_1$ and $\mathbf{D}_2$ are two 6×1 constant column matrices to be determined from boundary conditions, and $\mathbf{I}$ is the 6×6 unit matrix.

From Eq. (18), the constant column matrices $\mathbf{D}_1$ and $\mathbf{D}_2$ for the jth layer can be derived as

$$\begin{bmatrix}\mathbf{D}_1\\ \mathbf{D}_2\end{bmatrix}_j=\left\langle \mathrm{e}^{-s^*(z-z_j)}\right\rangle\begin{bmatrix}\mathbf{A}_1 & \mathbf{A}_2\\ \mathbf{B}_1 & \mathbf{B}_2\end{bmatrix}^{-1}\begin{bmatrix}\mathbf{I} & \mathbf{0}\\ \mathbf{0} & \mathrm{e}^{-\eta(z-z_j)}\mathbf{I}\end{bmatrix}\begin{bmatrix}\mathbf{u}\\ \mathbf{t}\end{bmatrix}_j. \tag{20}$$

For the lower surface z_j and upper surface z_{j+1} of the jth layer, we have

$$\begin{bmatrix}\mathbf{D}_1\\ \mathbf{D}_2\end{bmatrix}_j=\begin{bmatrix}\mathbf{A}_1 & \mathbf{A}_2\\ \mathbf{B}_1 & \mathbf{B}_2\end{bmatrix}^{-1}\begin{bmatrix}\mathbf{u}\\ \mathbf{t}\end{bmatrix}_{z_j}=\left\langle \mathrm{e}^{-s^* h_j}\right\rangle\begin{bmatrix}\mathbf{A}_1 & \mathbf{A}_2\\ \mathbf{B}_1 & \mathbf{B}_2\end{bmatrix}^{-1}\begin{bmatrix}\mathbf{I} & \mathbf{0}\\ \mathbf{0} & \mathrm{e}^{-\eta h_j}\mathbf{I}\end{bmatrix}\begin{bmatrix}\mathbf{u}\\ \mathbf{t}\end{bmatrix}_{z_{j+1}}. \tag{21}$$

Therefore, the physical quantities at the upper surface z_{j+1} can be expressed in terms of those at the lower surface z_j as

$$\begin{bmatrix}\mathbf{u}\\ \mathbf{t}\end{bmatrix}_{z_{j+1}}=\begin{bmatrix}\mathbf{I} & \mathbf{0}\\ \mathbf{0} & \mathrm{e}^{\eta h_j}\mathbf{I}\end{bmatrix}\begin{bmatrix}\mathbf{A}_1 & \mathbf{A}_2\\ \mathbf{B}_1 & \mathbf{B}_2\end{bmatrix}\left\langle \mathrm{e}^{s^* h_j}\right\rangle\begin{bmatrix}\mathbf{A}_1 & \mathbf{A}_2\\ \mathbf{B}_1 & \mathbf{B}_2\end{bmatrix}^{-1}\begin{bmatrix}\mathbf{u}\\ \mathbf{t}\end{bmatrix}_{z_j}. \tag{22}$$

With the continuity condition of the displacement and traction components across the interfaces, the physical quantities at the bottom surface $z=0$ can propagate to any z-level ($0<z\le H$) of the nanoplate by using the propagator matrix repeatedly. Therefore, the extended displacement and traction vectors at any z-level can be derived as

$$\begin{bmatrix}\mathbf{u}\\ \mathbf{t}\end{bmatrix}_z=\mathbf{P}_j(z-z_j)\mathbf{P}_{j-1}(h_{j-1})\ldots\mathbf{P}_2(h_2)\mathbf{P}_1(h_1)\begin{bmatrix}\mathbf{u}\\ \mathbf{t}\end{bmatrix}_0 \tag{23}$$

where the propagator matrix $\mathbf{P}_j(h_j)$ is

$$\mathbf{P}_j(h_j)=\begin{bmatrix}\mathbf{I} & \mathbf{0}\\ \mathbf{0} & \mathrm{e}^{\eta h_j}\mathbf{I}\end{bmatrix}\begin{bmatrix}\mathbf{A}_1 & \mathbf{A}_2\\ \mathbf{B}_1 & \mathbf{B}_2\end{bmatrix}\left\langle \mathrm{e}^{s^* h_j}\right\rangle\begin{bmatrix}\mathbf{A}_1 & \mathbf{A}_2\\ \mathbf{B}_1 & \mathbf{B}_2\end{bmatrix}^{-1}. \tag{24}$$

Consider a layered nanoplate subjected to a z-direction uniformly distributed patch loading on its top surface, and all other traction boundary conditions at the top and bottom surfaces are zero, i.e.,

$$\begin{cases}\mathbf{t}(H)=\left[\sigma_{xz},\sigma_{yz},\sigma_{zz},H_{xz},H_{yz},D_z\right]^{\mathrm{T}}=[0,0,f(x,y),0,0,0]^{\mathrm{T}}\\ \mathbf{t}(0)=\mathbf{0}\end{cases}, \tag{25}$$

where the loading function $f(x,y)$ can be approximately written in a dual Fourier series expansion as

$$f(x,y)\approx\sum_{m=1}^{M}\sum_{n=1}^{N}a_{mn}\sin px\sin qy \tag{26}$$

with a_{mn} being the loading coefficients, and they take the form as [47]

$$a_{mn}=\frac{4}{L_x L_y}\int_0^{L_x}\int_0^{L_y}f(x,y)\sin px\sin qy\mathrm{d}x\mathrm{d}y. \tag{27}$$

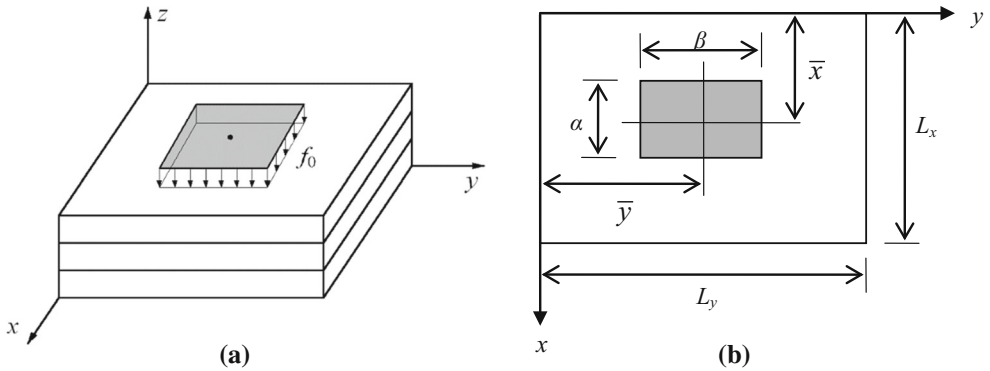

Fig. 2 **a** FG layered 2D QC nanoplate subjected to patch loading. **b** Vertical view of rectangular patch loading in $x - y$ plane

For the uniformly distributed patch loading with intensity f_0 over an area of $\alpha \times \beta$ located at $(\bar{x}, \bar{y})$, as shown in Fig. 2, the loading coefficients a_{mn} can be rewritten as

$$a_{mn} = \frac{16 f_0}{\pi^2 mn} \sin p\bar{x} \sin q\bar{y} \sin \frac{p\alpha}{2} \sin \frac{q\beta}{2}. \tag{28}$$

A uniform loading is a special case for patch loading in which the loading coefficients a_{mn} can be obtained when $\alpha \times \beta = L_x \times L_y$.

The exact solution in Eq. (23), when the z-level is replaced by the top surface $z = H$ of the nanoplate, can be recast into the following form:

$$\begin{bmatrix} \mathbf{u}(H) \\ \mathbf{t}(H) \end{bmatrix} = \begin{bmatrix} \mathbf{C}_1 & \mathbf{C}_2 \\ \mathbf{C}_3 & \mathbf{C}_4 \end{bmatrix} \begin{bmatrix} \mathbf{u}(0) \\ \mathbf{0} \end{bmatrix} \tag{29}$$

where $\mathbf{C}_1$, $\mathbf{C}_2$, $\mathbf{C}_3$, and $\mathbf{C}_4$ are the submatrices of the propagator matrix.

The unknown displacements at the bottom and top surfaces of the layered nanoplate are derived in terms of Eqs. (25) and (29) as

$$\mathbf{u}(0) = \mathbf{C}_3^{-1}\mathbf{t}(H), \quad \mathbf{u}(H) = \mathbf{C}_1\mathbf{C}_3^{-1}\mathbf{t}(H). \tag{30}$$

4 Numerical examples

Numerical results are presented to illustrate the size-dependent behavior of simply supported FG multilayered nanoplates subjected to a top surface patch loading with an intensity $f_0 = -1$ N/m^2. The center of patch loading is located at $(\bar{x}, \bar{y}) = (L_x/2, L_y/2)$, and the appropriate M and N in Eq. (26) are taken to ensure the series expansion truncation error for patch loadings less than 1%. The horizontal dimensions of the nanoplates are $L_x \times L_y = 50$ nm $\times$ 50 nm, and the total thickness for a single nanoplate is 3 nm. As for the layered nanoplates modeling with three layers, each layer has an equal thickness of 1 nm. The stacking sequence of the FG multilayered nanoplates is $BaTiO_3$/Al–Ni–Co/$BaTiO_3$ (called C/QC/C) and Al–Ni–Co/$BaTiO_3$/Al–Ni–Co (called QC/C/QC), respectively. The influences of patch size and nonlocal parameter on a single FG QC nanoplate are numerically investigated, and the effect of the stacking sequence on the FG layered nanoplates is also studied.

The material properties for the crystal $BaTiO_3$ are listed in Table 1 [48]. Because it is difficult to measure the piezoelectric and permittivity constants for 2D piezoelectric QCs, therefore 0.5 times piezoelectric constant and 2 times permittivity constant of $BaTiO_3$ are taken for them. The material properties for the QC alloy Al–Ni–Co are listed in Table 2 [5]. In order to avoid singular matrices during calculation, the crystals $BaTiO_3$ are regarded as special QCs, and approximately 10^{-8} of the corresponding K_i value in the QC layer is taken for the crystal layer.

4.1 Influence of patch size on a single FG nanoplate

In order to investigate the effect of patch size on a single FG nanoplate, the patch loading area is taken as $\alpha \times \beta = 0.5L_x \times 0.5L_y$, $0.7L_x \times 0.7L_y$ and $1.0L_x \times 1.0L_y$, respectively. Both nonlocal parameter l and exponential factor η are equal to 2.

Table 1 Material properties of $BaTiO_3$

Phonon elastic coefficients ($\times 10^9$ N/m^2)					
$C_{11}^0 = 166$	$C_{12}^0 = 77$	$C_{13}^0 = 78$	$C_{33}^0 = 162$	$C_{44}^0 = 43$	$C_{66}^0 = 44.5$
Piezoelectric constants (C/m^2)			Permittivity constants ($\times 10^{-9}$ C^2/(N m^2))		
$e_{15}^0 = 11.6$	$e_{31}^0 = -4.4$	$e_{33}^0 = 18.6$ $d_{112}^0 = 0$	$\kappa_{11}^0 = \kappa_{22}^0 = 11.2$	$\kappa_{33}^0 = 12.6$	

Table 2 Material properties of Al-Ni-Co

Phonon elastic coefficients ($\times 10^9$ N/m^2)					
$C_{11}^0 = 234.3$	$C_{12}^0 = 57.4$	$C_{13}^0 = 66.6$	$C_{33}^0 = 232.2$	$C_{44}^0 = 70.2$	$C_{66}^0 = 88.5$
Phonon–phason coupling coefficients ($\times 10^9$ N/m^2)			Phason elastic coefficients ($\times 10^9$ N/m^2)		
$R_1^0 = 8.85$			$K_1^0 = 122$	$K_2^0 = 24$	$K_4^0 = 12$
Piezoelectric constants (C/m^2)			Permittivity constants ($\times 10^{-9}$ C^2/(N·m^2))		
$e_{15}^0 = 5.8 e_{31}^0 = -2.2 e_{33}^0 = 9.3 d_{112}^0 = 0$			$\kappa_{11}^0 = \kappa_{22}^0 = 22.4 \kappa_{33}^0 = 25.2$		

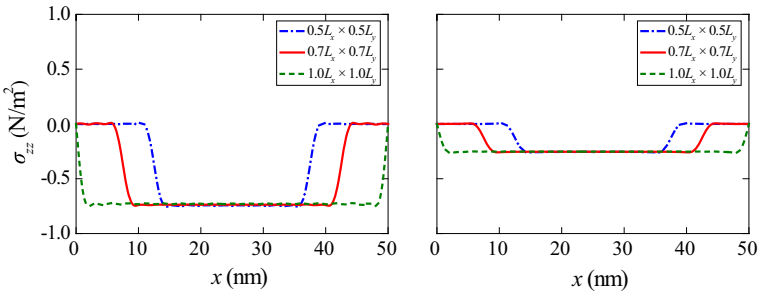

Fig. 3 Effect of patch size on phonon stress σ_{zz} along lateral x-direction in a single FG nanoplate. **a** σ_{zz} at $z = 2$ nm. **b** σ_{zz} at $z = 1$ nm

Figure 3a, b shows the distribution of phonon stress σ_{zz} along lateral x-direction in the fixed vertical plane at $y = 0.5L_y$ with $z = 2$ nm and 1 nm, respectively. The value of σ_{zz} outside the scope of the loading is zero, and its maximum value under patch load area is not sensitive to patch size. Furthermore, σ_{zz} at $z = 2$ nm in Fig. 3a is larger than that at $z = 1$ nm in Fig. 3b on account of the top surface loading.

Figure 4 presents the variations of phonon and phason stresses for different patch sizes along the z-direction of the nanoplate. The influence of patch loading area on the following induced physical quantities along the z-direction in this Subsection is shown at the fixed horizontal coordinates $(x/L_x, y/L_y) = (0.4, 0.4)$. The small influence of patch loading area on phonon stress σ_{zz} is observed from Fig. 4a, because of the same applied load on the top surface of the nanoplate, and the similar effect of it can be also found from phonon stress σ_{yz} (Fig. 4b). The in-plane phonon stresses σ_{xx} and σ_{xy} shown in Fig. 4c, d display a different trend with the out-plane stresses $\sigma_{zz}$and σ_{yz}, and their magnitudes increase as the patch size increases. Comparing with the influence of patch size on σ_{yz}, it is more obvious on phason stress H_{yz} (Fig. 4e). Phason stress H_{xx} (Fig. 4f) depending on patch size follows the similar trend with the in-plane phonon stresses. σ_{xx}, σ_{xy}, and H_{xx} are zero at the middle of the nanoplate owing to geometry symmetry about the z-axis.

Figure 5 depicts the dependence of phonon displacement u_z and phason displacement w_x along the z-direction on patch size, and the effect of it on the electric potential ϕ and electric displacements is shown in Fig. 6. u_z in Fig. 5a and ϕ in Fig. 6a increase with increasing patch loading area, and a similar trend can be observed from Fig. 5b for w_x. Not only that, w_x is nearly anti-symmetry with respect to $z = 1.5$ nm, which is somewhat similar to the behavior of H_{xx}. The electric displacements D_z (Fig. 6b) and D_y (Fig. 6d) are not very sensitive to patch size, whereas the electric displacement D_x (Fig. 6c) is dependent on it. In addition, the

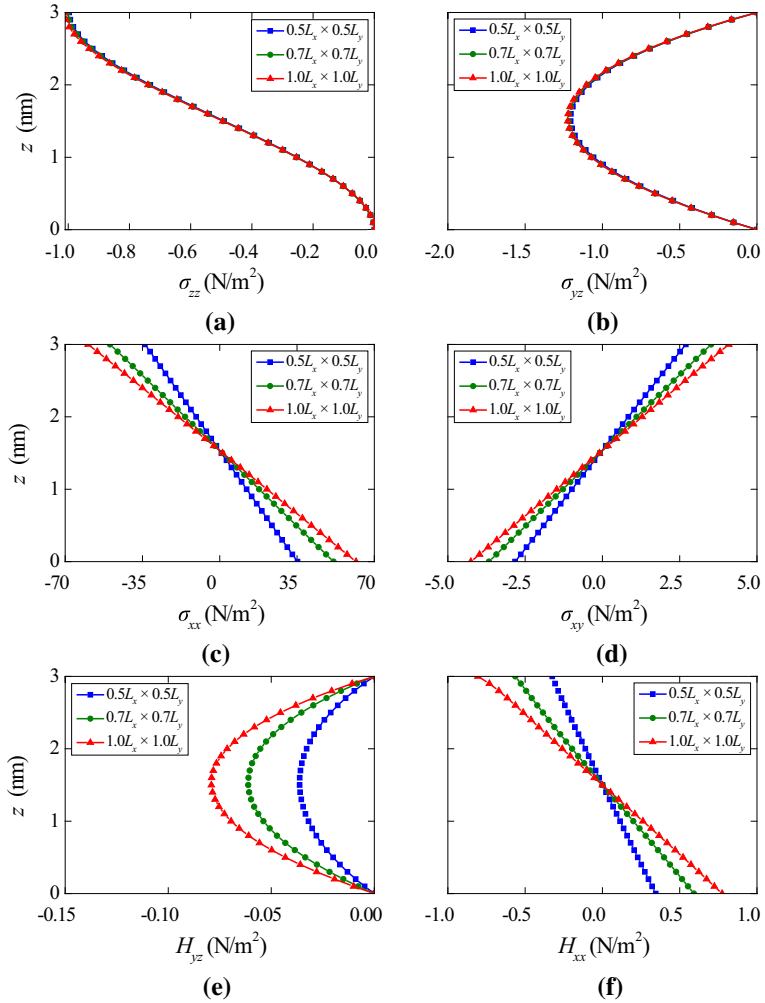

Fig. 4 Effect of patch size on phonon and phason stresses along the z-direction in a single FG nanoplate. **a** σ_{zz}. **b** σ_{yz}. **c** σ_{xx}. **d** σ_{xy}. **e** H_{yz}. **f** H_{xx}

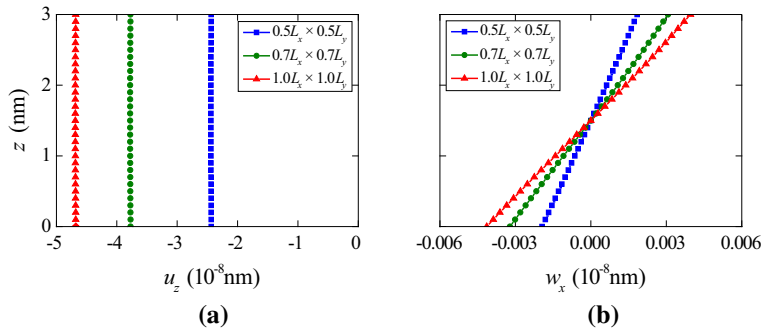

Fig. 5 Effect of patch size on phonon and phason displacements along the z-direction in a single FG nanoplate. **a** u_z. **b** w_x

maximum value of ϕ for a given patch size occurs at the middle of the nanoplate, whereas the value of D_z at the same z-level is nearly zero.

The satisfaction of the boundary conditions at the top and bottom surfaces can be observed from phonon stresses σ_{zz}, σ_{yz}, phason stress H_{yz}, and electric displacement D_z, which can partly demonstrate the exactness of the obtained solution.

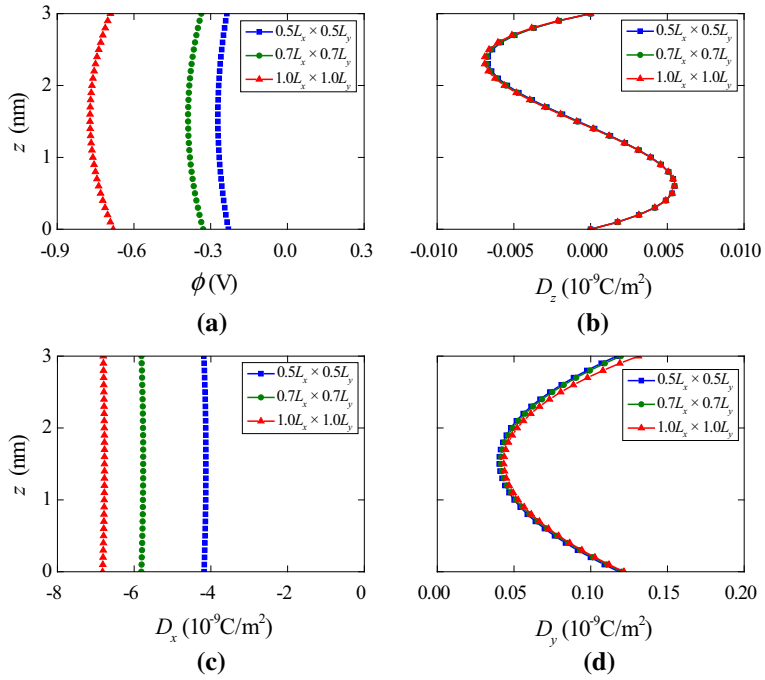

Fig. 6 Effect of patch size on electric potential and electric displacements along the z-direction in a single FG nanoplate. **a** ϕ. **b** D_z. **c** D_x. **d** D_y

4.2 Influence of the nonlocal parameter on a single FG nanoplate

The responses of a single FG nanoplate with different nonlocal parameters are investigated in this Subsection. The nonlocal parameter is taken in the conservative range of l = 0, 1, 2 nm [33]. The patch loading area is $\alpha \times \beta = L_x \times L_y$, and the exponential factor η is selected as 2. The induced physical quantities along the thickness of the nanoplate are shown at the fixed horizontal coordinates $(x/L_x, y/L_y)$ = (0.15, 0.15).

Figure 7 shows the variation of the stress components in the phonon and phason fields along the z-direction for different nonlocal parameters l. The out-plane phonon stresses σ_{zz} and σ_{yz} in Fig. 7a, b are almost independent of l, while the relatively obvious effect of l on the in-plane stresses σ_{xx} and σ_{xy} in Fig. 7c, d is found. Moreover, σ_{xx} and σ_{xy} increase with decreasing l. There is nearly no influence of l on phason stress H_{yz} (Fig. 7e), which is similar to the trend of out-plane phonon stresses with respect to l. By comparing the effect of l on H_{yz}, the quite overt response of in-plane phason stress H_{xx} is seen in Fig. 7f.

The effect of nonlocal parameter l on displacements, electric potential, and electric displacements is shown in Figs. 8 and 9, respectively. The noticeable changes induced by different l are presented in Fig. 8a for phonon displacement u_z, in Fig. 9a for electric potential ϕ, and they increase with increasing l. Similar to the trend of u_z, l has a significant influence on phason displacement w_x in Fig. 8b. Due to the geometry symmetry about the z-axis, w_x is zero at the middle of the nanoplate. Electric displacement D_z (Fig. 9b) is nearly independent of l, while the dependence of electric displacements D_x (Fig. 9c) and D_y (Fig. 9d) on l is obvious. Furthermore, the maximum values of ϕ, D_x, and D_y appear at the middle of the nanoplate.

4.3 Influence of stacking sequence on FG layered nanoplates

Considering FG sandwich nanoplates with two stacking sequences (i.e., QC/C/QC and C/QC/C) subjected to a uniform loading on their top surfaces, the effect of stacking sequence on the nanoplates is studied. The nonlocal parameter is $l = 2$, and the exponential factor is taken as $\eta = 2$. The responses of the physical quantities along the z-direction of the FG multilayered nanoplates are also fixed at horizontal coordinates $(x/L_x, y/L_y)$ = (0.15, 0.15).

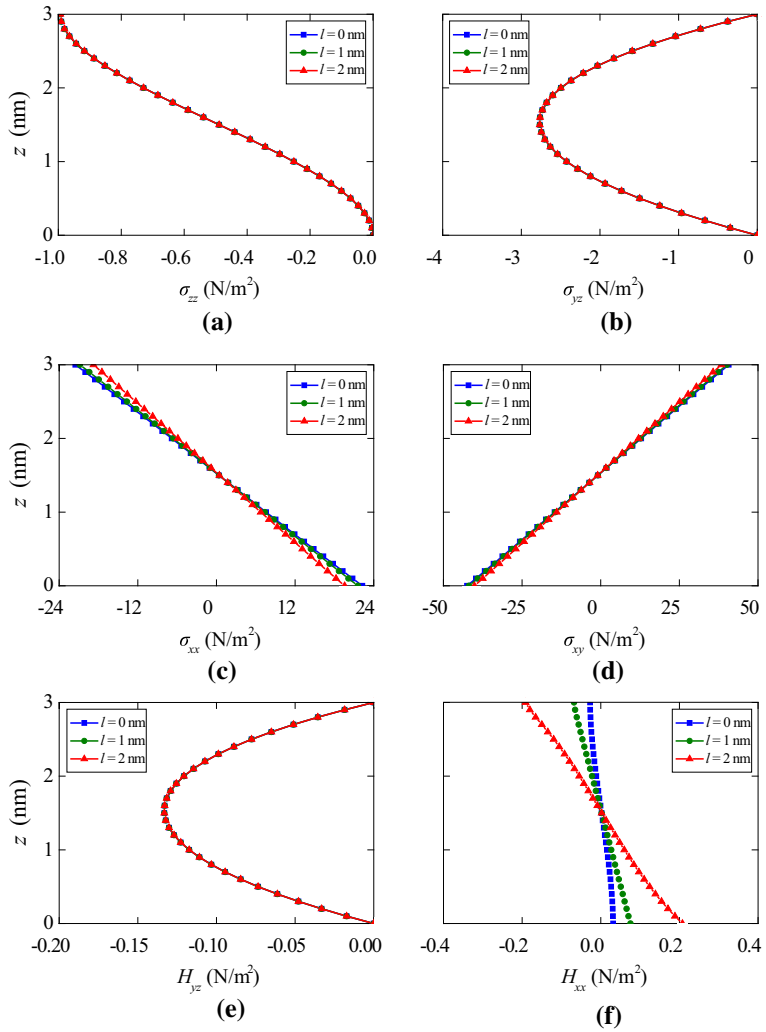

Fig. 7 Effect of the nonlocal parameter on phonon and phason stresses along the z-direction in a single FG nanoplate. **a** σ_{zz}. **b** σ_{yz}. **c** σ_{xx}. **d** σ_{xy}. **e** H_{yz}. **f** H_{xx}

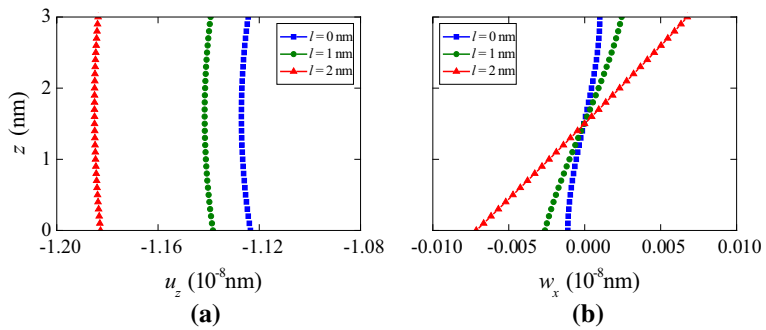

Fig. 8 Effect of the nonlocal parameter on phonon and phason displacements along the z-direction in a single FG nanoplate. **a** u_z. **b** w_x

The effect of stacking sequence on phonon and phason stresses is presented in Fig. 10. The value of phonon stress σ_{zz} (Fig. 10a) is -1 at the top surfaces, and zero at the bottom surfaces of the nanoplates, and phonon stress σ_{yz} (Fig. 10b) and phason stress H_{yz} (Fig. 10e) are zero at the top and bottom surfaces, so they satisfy the boundary conditions. The different behaviors of σ_{zz} and σ_{yz} are induced by different stacking sequences

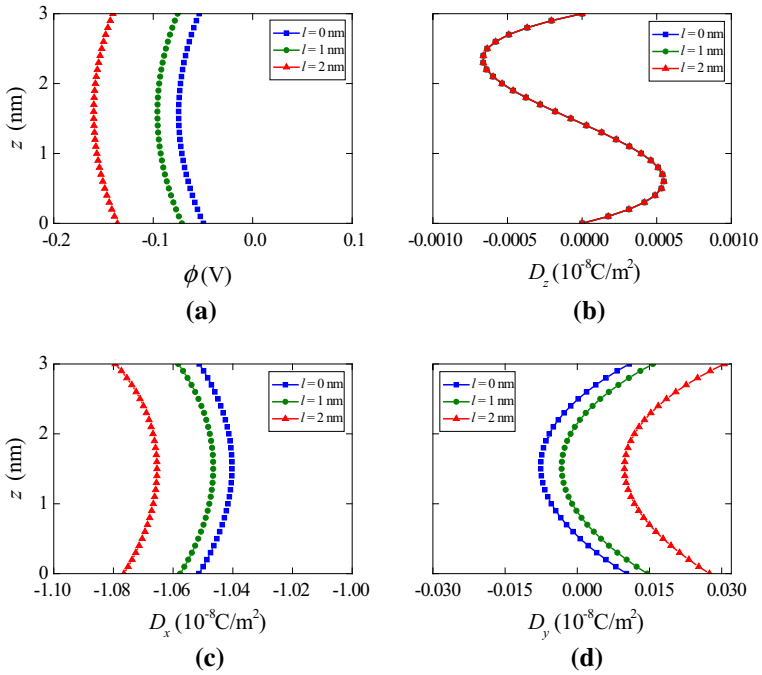

Fig. 9 Effect of the nonlocal parameter on electric potential and electric displacements along the z-direction in a single FG nanoplate. **a** ϕ. **b** D_z. **c** D_x. **d** D_y

due to the change of the material properties. Furthermore, σ_{zz} and σ_{yz} are continuous at the interfaces of the layers, which meets the agreement with continuity boundary condition. σ_{yz} in QC/C/QC nanoplate is smaller than that in C/QC/C nanoplate. The significant feature means that QCs are expected to be used as the surface layer of the sandwich nanoplates, which may be related to the high wear resistance of QCs. The discontinuous phonon stresses σ_{xx} and σ_{xy} in Fig. 10c, d appear at the interfaces of the layers, and the discontinuity of σ_{xx} in QC/C/QC nanoplate is a little bit smaller than that in C/QC/C nanoplate. Compared with the phonon stresses, the smaller phason stresses H_{yz} and H_{xy} (Fig. 10f) are induced. Furthermore, H_{yz} and H_{xy} are sensitive to stacking sequence, and they are zero in the crystal layer due to no phason fields in the crystal.

Figures 11 and 12 show, respectively, the variation of phonon displacement, phason displacement, electric potential, and electric displacements along the thickness direction of the nanoplates with different stacking sequences. The stacking sequence has a conspicuous influence on all physical quantities in the displacement and electric fields. u_z (Fig. 11a) in C/QC/C nanoplate is larger than that in QC/C/QC nanoplate, and they are continuous at the interfaces of the layers. The atomic rearrangement does not occur in crystals, so the phason displacement in the crystal layer is zero. Moreover, the maximum values of w_x appear at the top and bottom surfaces of the layered nanoplates. The continuous behavior like u_z is also found for electric potential ϕ (Fig. 12a) and z-direction electric displacement D_z (Fig. 12b), while a similar trend does not exist in electric displacements D_x (Fig. 12c) and D_y (Fig. 12d). The maximum value of ϕ for any sandwich nanoplates appears at the middle layer, whereas the maximum value for D_z occurs at the interfaces of the layers. The discontinuity of D_x in QC/C/QC nanoplates is relatively smaller than that in C/QC/C nanoplates, and D_y follows a similar trend. Therefore, QC/C/QC nanoplates can be selected as engineering structural materials to reduce the discontinuity at the interfaces.

5 Conclusions

The static deformation of the simply supported FG multilayered 2D QC nanoplates subjected to patch loading on their top surfaces is analyzed. The exact solution is achieved on the basis of the extended nonlocal elastic theory, pseudo-Stroh formalism, and propagator matrix method. Typical numerical examples presented have shown the noticeable influences of patch size, nonlocal parameter, and stacking sequence on the nanoplates.

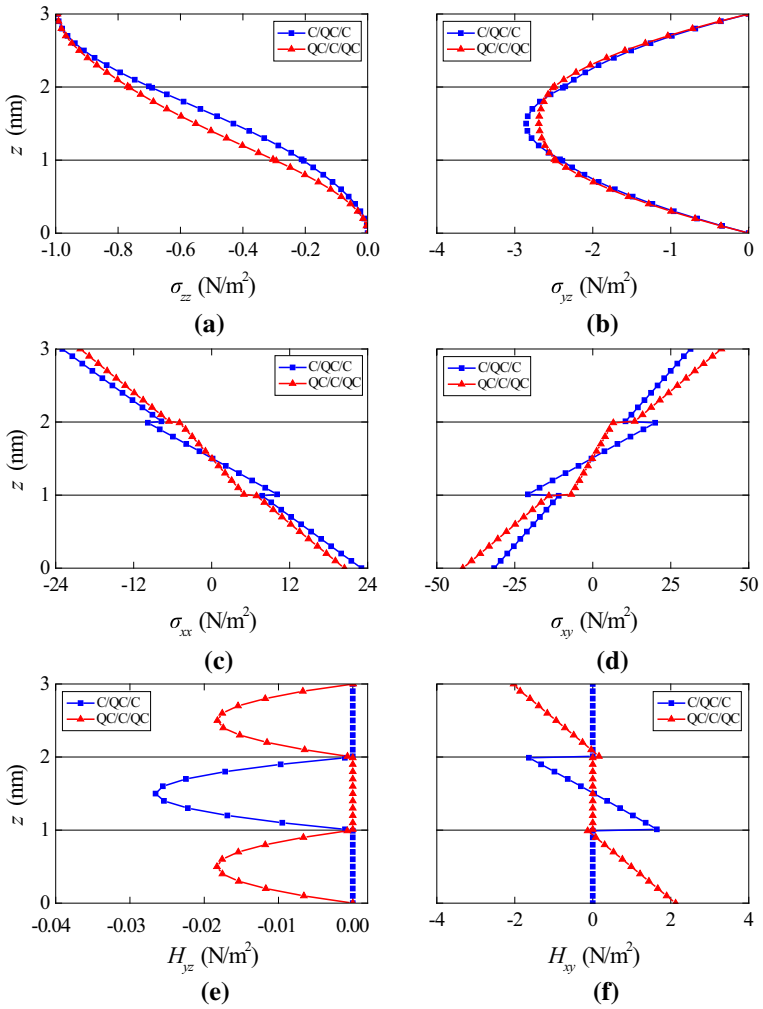

Fig. 10 Effect of stacking sequence on phonon and phason stresses along the z-direction in the FG layered nanoplates. **a** σ_{zz}. **b** σ_{yz}. **c** σ_{xx}. **d** σ_{xy}. **e** H_{yz}. **f** H_{xy}

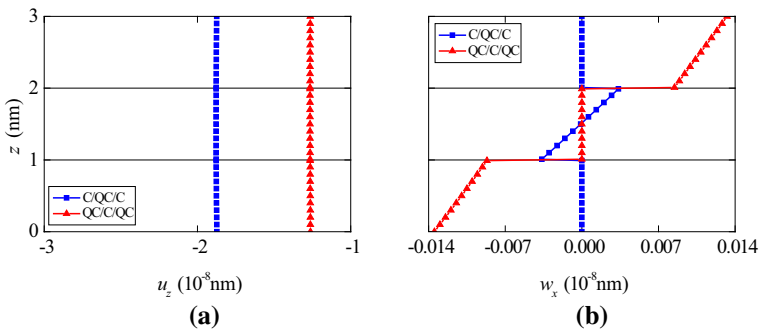

Fig. 11 Effect of stacking sequence on phonon and phason displacements along the z-direction in the FG-layered nanoplates. **a** u_z. **b** w_x

The in-plane phonon and phason stresses, phonon and phason displacements, electric potential, and in-plane electric displacements are sensitive to patch size and nonlocal parameter. The stacking sequence has a pronounced effect on almost all physical quantities at any z-level (including the surfaces and interfaces) of the nanoplates. Furthermore, the smaller phonon stresses and displacement are induced in QC/C/QC nanoplates, which can promote the application of QCs as surface coatings. The results of the current study can be used to

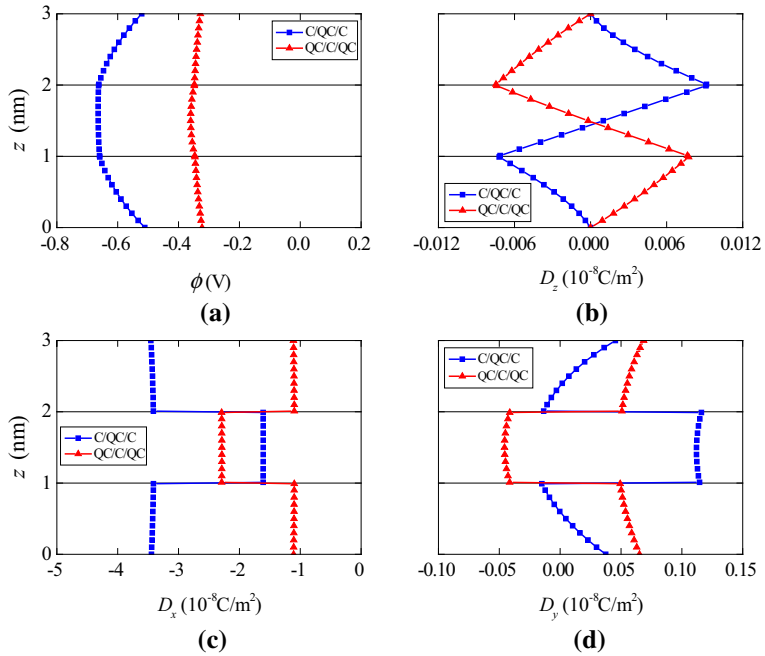

Fig. 12 Effect of stacking sequence on electric potential and electric displacements along the z-direction in the FG-layered nanoplates. **a** ϕ. **b** D_z. **c** D_x. **d** D_y

validate the accuracy of other numerical methods, and serve as benchmarks in the design for the FG layered nanoplates made of QCs.

Acknowledgements The work is supported by the National Natural Science Foundation of China (Nos. 11472299 and 51704015) and China Agricultural University Education Foundation (No. 1101-240001).

References

1. Shechtman, D., Blech, I., Gratias, D., Cahn, J.W.: Metallic phase with long-range orientational order and no translational symmetry. Phys. Rev. Lett. **53**(20), 1951–1953 (1984)
2. Levine, D., Steinhardt, P.J.: Quasicrystals: a new class of ordered structures. Phys. Rev. Lett. **53**(26), 2477–2480 (1984)
3. Ding, D.H., Yang, W.G., Hu, C.Z., Wang, R.H.: Generalized elasticity theory of quasicrystals. Phys. Rev. B **48**(10), 7003–7010 (1993)
4. Fan, T.Y.: Mathematical theory of elasticity of quasicrystals and its applications. Springer, Heidelberg (2011)
5. Yang, L.Z., Gao, Y., Pan, E., Waksmanski, N.: An exact solution for a multilayered two-dimensional decagonal quasicrystal plate. Int. J. Solids Struct. **51**(9), 1737–1749 (2014)
6. Louzguine-Luzgin, D.V., Inoue, A.: Formation and properties of quasicrystals. Ann. Rev. Mater. Res. **38**, 403–423 (2008)
7. Dubois, J.M., Kang, S.S., Vonstebut, J.: Quasicrystalline low-friction coatings. J. Mater. Sci. Lett. **10**(9), 537–541 (1991)
8. Zhang, L.L., Zhang, Y.M., Gao, Y.: General solutions of plane elasticity of one-dimensional orthorhombic quasicrystals with piezoelectric effect. Phys. Lett. A **378**(37), 2768–2776 (2014)
9. Li, L.H., Liu, G.T.: Stroh formalism for icosahedral quasicrystal and its application. Phys. Lett. A **376**(8–9), 987–990 (2012)
10. Hu, C.Z., Wang, R.H., Ding, D.H., Yang, W.G.: Piezoelectric effects in quasicrystals. Phys. Rev. B **56**(5), 2463–2468 (1997)
11. Wu, D., Zhang, L.L., Xu, W.S., Yang, L.Z., Gao, Y.: Electroelastic Green's function of one-dimensional piezoelectric quasicrystals subjected to multi-physics loads. J. Int. Syst. Struct. **28**(12), 1651–1661 (2017)
12. Gao, Y., Ricoeur, A., Zhang, L.L., Yang, L.Z.: Crack solutions and weight functions for plane problems in three-dimensional quasicrystals. Arch. Appl. Mech. **84**(8), 1103–1115 (2014)
13. Guo, X.P., Chen, J.F., Yu, H.L., Liao, H.L., Coddet, C.: A study on the microstructure and tribological behavior of cold-sprayed metal matrix composites reinforced by particulate quasicrystal. Surf. Coat. Technol. **268**, 94–98 (2015)
14. Guo, J.H., Yu, J., Xing, Y.M., Pan, E., Li, L.H.: Thermoelastic analysis of a two-dimensional decagonal quasicrystal with a conductive elliptic hole. Acta Mech. **227**(9), 2595–2607 (2016)
15. Gao, Y., Ricoeur, A., Zhang, L.L.: Plane problems of cubic quasicrystal media with an elliptic hole or a crack. Phys. Lett. A **375**(28), 2775–2781 (2011)
16. Gao, Y., Yu, L.Y., Yang, L.Z., Zhang, L.L.: The refined theory of 2D quasicrystal deep beams based on elasticity of quasicrystals. Struct. Eng. Mech. **53**(3), 411–427 (2015)
17. Guo, J.H., Pan, E.: Three-phase cylinder model of one-dimensional hexagonal piezoelectric quasi-crystal composites. J. Appl. Mech. **83**(8), 081007 (2016)

18. Waksmanski, N., Pan, E., Yang, L.Z., Gao, Y.: Free vibration of a multilayered one-dimensional quasi-crystal plate. J. Vib. Acoust. **136**(4), 041019 (2014)
19. Yang, L.Z., Li, Y., Gao, Y., Pan, E., Waksmanski, N.: Three-dimensional exact electric-elastic analysis of a multilayered two-dimensional decagonal quasicrystal plate subjected to patch loading. Compos. Struct. **171**, 198–216 (2017)
20. Yang, L.Z., Gao, Y., Pan, E., Waksmanski, N.: An exact closed-form solution for a multilayered one-dimensional orthorhombic quasicrystal plate. Acta Mech. **226**(11), 3611–3621 (2015)
21. Li, X.Y., Li, P.D.: Three-dimensional thermo-elastic general solutions of one-dimensional hexagonal quasi-crystal and fundamental solutions. Phys. Lett. A **376**(26–27), 2004–2009 (2012)
22. Li, X.Y., Li, P.D., Wu, T.H., Shi, M.X., Zhu, Z.W.: Three-dimensional fundamental solutions for one-dimensional hexagonal quasicrystal with piezoelectric effect. Phys. Lett. A **378**(10), 826–834 (2014)
23. Fan, C.Y., Yuan, Y.P., Pan, Y.B., Zhao, M.H.: Analysis of cracks in one-dimensional hexagonal quasicrystals with the heat effect. Int. J. Solids Struct. **120**, 146–156 (2017)
24. Li, L.H., Liu, G.T.: Decagonal quasicrystal plate with elliptic holes subjected to out-of-plane bending moments. Phys. Lett. A **378**(10), 839–844 (2014)
25. Sladek, J., Sladek, V., Pan, E.: Bending analyses of 1D orthorhombic quasicrystal plates. Int. J. Solids Struct. **50**(24), 3975–3983 (2013)
26. Waksmanski, N., Pan, E., Yang, L.Z., Gao, Y.: Harmonic response of multilayered one-dimensional quasicrystal plates subjected to patch loading. J. Sound Vib. **375**, 237–253 (2016)
27. Inoue, A.: Amorphous, nanoquasicrystalline and nanocrystalline alloys in Al-based systems. Prog. Mater. Sci. **43**(5), 365–520 (1998)
28. Schurack, F., Eckert, J., Schultz, L.: High strength AL-alloys with nanoquasicrystalline phase as main component. Nanostruct. Mater. **12**(1), 107–110 (1999)
29. Eringen, A.C.: On differential equations of nonlocal elasticity and solutions of screw dislocation and surface waves. J. Appl. Phys. **54**(9), 4703–4710 (1983)
30. Despotovic, N.: Stability and vibration of a nanoplate under body force using nonlocal elasticity theory. Acta Mech. **229**(1), 273–284 (2018)
31. Barati, M.R.: Vibration analysis of porous FG nanoshells with even and uneven porosity distributions using nonlocal strain gradient elasticity. Acta Mech. **229**(3), 1183–1196 (2018)
32. Guo, J.H., Chen, J.Y., Pan, E.N.: Free vibration of three-dimensional anisotropic layered composite nanoplates based on modified couple-stress theory. Physica E **87**, 98–106 (2017)
33. Pan, E., Waksmanski, N.: Deformation of a layered magnetoelectroelastic simply-supported plate with nonlocal effect, an analytical three-dimensional solution. Smart Mater. Struct. **25**(9), 095013 (2016)
34. Waksmanski, N., Pan, E.: Nonlocal analytical solutions for multilayered one-dimensional quasicrystal nanoplates. J. Vib. Acoust. **139**(2), 021006 (2017)
35. Ma, L.H., Ke, L.L., Wang, Y.Z., Wang, Y.S.: Wave propagation in magneto-electro-elastic nanobeams via two nonlocal beam models. Physica E **86**, 253–261 (2017)
36. Reddy, J.N.: Nonlocal theories for bending, buckling and vibration of beams. Int. J. Eng. Sci. **45**(2–8), 288–307 (2007)
37. Li, Y., Yang, L.Z., Gao, Y.: An exact solution for a functionally graded multilayered one-dimensional orthorhombic quasicrystal plate (2017). https://doi.org/10.1007/s00707-017-2028-8
38. Koizumi, M.: FGM activities in Japan. Compos. Part B **28**(1–2), 1–4 (1997)
39. Guo, J.H., Chen, J.Y., Pan, E.: Size-dependent behavior of functionally graded anisotropic composite plates. Int. J. Eng. Sci. **106**, 110–124 (2016)
40. Daneshmehr, A., Rajabpoor, A., Pourdavood, M.: Stability of size dependent functionally graded nanoplate based on nonlocal elasticity and higher order plate theories and different boundary conditions. Int. J. Eng. Sci. **82**, 84–100 (2014)
41. Ke, L.L., Liu, C., Wang, Y.S.: Free vibration of nonlocal piezoelectric nanoplates under various boundary conditions. Physica E **66**, 93–106 (2015)
42. Chan, K.C., Qu, N.S., Zhu, D.: Fabrication of graded nickel-quasicrystal composite by electrodeposition. Trans. Inst. Met. Finish. **80**, 210–213 (2002)
43. Dubois, J.M.: Useful Quasicrystals. World Scientific, Singapore (2005)
44. Pan, E.: Exact solution for simply supported and multilayered magneto-electro-elastic plates. J. Appl. Mech. **68**(4), 608–618 (2001)
45. Altay, G., Dökmeci, M.C.: On the fundamental equations of piezoelasticity of quasicrystal media. Int. J. Solids Struct. **49**(23–24), 3255–3262 (2012)
46. Jha, D.K., Kant, T., Singh, R.K.: A critical review of recent research on functionally graded plates. Compos. Struct. **96**, 833–849 (2013)
47. Timoshenko, S., Woinowsky-Krieger, S.: Theory of Plates and Shells. McGraw-Hill Book Company, New York (1959)
48. Lee, J.S., Jiang, L.Z.: Exact electroelastic analysis of piezoelectric laminae via state space approach. Int. J. Solids Struct. **33**(7), 977–990 (1996)